ACTIVE JAMMING CANCELLATION CONCEPT FOR EXTENDED RANGE GUIDED MUNITIONS

Mr. George C. Wiles IV, Mr. Ernest J. Ohlmeyer, Dr. Thomas R. Pepitone, Mr. Gary L. Sitzman, Mr. B. Larry Miller, and Ms. Paula K. Khoe

The Extended Range Guided Munition (ERGM) design philosophy focuses on in-flight calibration of inertial measurement unit (IMU) bias errors early in the flight in anticipation of enemy jamming and possible loss of Global Positioning System (GPS) aiding in the vicinity of the target area. To further mitigate the effects of jamming, ERGM also employs antijam and interference cancellation features. This article assesses the performance of a tightly-coupled GPS-aided inertial navigation system (GPS/INS) and a conceptual active antijam system in the context of typical ERGM scenarios. A generic model of an antenna interference cancellation system was developed to provide a means of predicting the navigation system's dual antenna performance in the presence of jamming. Simulated performance data are presented depicting the behavior of the antijam system with respect to jammer power, frequency, polarization, and trajectory geometry. The interference cancellation model was also embedded in a GPS/INS navigation simulation and evaluated along two representative ERGM trajectories. The analysis assumed an early developmental ERGM configuration that differs from the final tactical design. Results for 40- and 60-nautical mile (NM) trajectories showed that the interference cancellation system provided good antijam immunity until very late in the trajectory in a severe jamming environment. GPS loss of lock occurred only seconds prior to impact, resulting in navigation system accuracies that were within desired values. These preliminary performance data suggest that the ERGM navigation system can meet system accuracy requirements in the presence of realistic levels of continuous wave (CW) and broadband jamming.

INTRODUCTION

GPS receivers exhibit several properties that make them potentially susceptible to interference from external sources of noise. The GPS antenna must encompass a wide field of view to receive signals from all satellites above the local horizon, resulting in a relatively low-gain antenna array. In addition, GPS satellite signal power is intentionally very low; as a result, small, man-portable jammers in the target area can have a significant impact on receiver signal-to-noise ratio to the point that the signal acquisition and tracking can be affected. One technique that has been used with some success to mitigate the interference effects on ground-based satellite receiving stations is employing a dual-antenna cancellation system. Similar

applications of noise suppression in the acoustic arena can be found in automobile, aircraft and helicopter cabin noise reduction via active noise cancellation techniques.

The ERGM, presently under development by the Navy, will incorporate an active radio frequency (RF) antijam system to improve its immunity to enemy jamming and thereby maintain very stringent navigation accuracy requirements. The specific characteristics of the ERGM Antijam Module are considered proprietary, and therefore, design details were not available for this study. The present description represents an entirely independent but parallel design approach, aimed at quantifying the potential benefits of a conceptual active interference cancellation system within the context of typical engagement scenarios. The analysis presented here used an early developmental version of the ERGM airframe (and notional scenarios) not associated with the final tactical system.

The ERGM is a 5-in-diameter, rocket-boosted, roll-stabilized guided projectile. It incorporates a tightly-coupled GPS/INS navigation system, which allows precise calibration of the inertial sensors early in flight in anticipation of intense enemy jamming in the target area. The Naval Surface Warfare Center, Dahlgren Division (NSWCDD) has independently developed generic models of the antijam portion of the system to integrate with the existing government ERGM 6 degree-of-freedom (6-DOF) simulation. This allows an independent assessment of navigation accuracy under a variety of jamming scenarios. This article represents an initial performance evaluation of a conceptual interference cancellation system in concert with a GPS/INS navigation system in a jamming environment.

In the following section, the fundamental properties of the RF cancellation system are discussed and illustrated in several figures. The equations constituting the noise cancellation algorithm are derived, and sample results are provided. Incorporation of canceller effectiveness into the computation of equivalent GPS carrier-to-noise ratio is also discussed. Extensions to the model are proposed that include the case of multiple jammers at arbitrary locations.

Next, the effectiveness of the canceller algorithm with respect to variations in jammer frequency, power, spectral distribution, polarization, and projectile/jammer geometry is addressed. Navigation accuracy is examined over two representative trajectories using a Monte Carlo navigation simulation. The ability to estimate and correct large initial alignment errors and IMU errors is evaluated. Terminal navigation accuracy expressed as 1-σ downrange and cross-range position errors at the target is determined. Particular attention is focused on the jamming immunity provided by the GPS antijam feature and the associated benefit to terminal navigation accuracy in the vicinity of the target.

INTERFERENCE CANCELLER ALGORITHM

Principle of Operation

In the dual-antenna cancellation system, a second antenna receives a scaled version of the unwanted jamming signal that is present at the primary or *signal* antenna. The canceller circuitry rescales and inverts the signal present in this secondary path to create an *antinoise* signal. This signal is added to the primary signal path where the noise and antinoise signals ideally cancel, leaving only the desired signal. On the ERGM projectile, the primary signal path is through a patch antenna mounted on the top of the roll-stabilized projectile oriented towards the satellites. The secondary path is through an identical patch mounted on the underside of the projectile. For the remainder of this article, the top antenna and associated components are referred to as the *signal* antenna or path, denoted by the subscript ***S***, and the bottom antenna and its components as the *jammer* antenna or path, denoted by the subscript ***J***.

A simplified diagram of a generic noise cancellation system is shown in Figure 1. P_J represents the jamming power incident on the two antenna patches. The complex gains G_S and G_J represent the gains associated with the signal and jammer paths, respectively, including the antenna, filtering, and preamplification. The frequency-dependent gains G_S and G_J are derived experimentally and determine the power admitted to each signal path. G_C

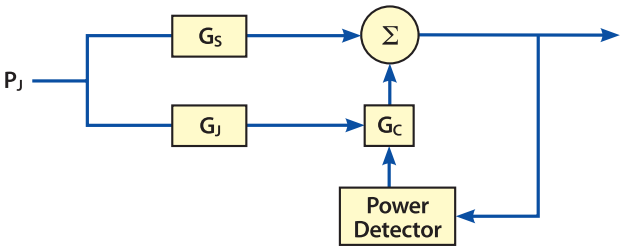

Figure 1—GPS Interference Canceller Conceptual Diagram

represents the complex gain of the canceller circuit, which is to be computed in such a way as to minimize the transmission of jammer power, P_J, to the signal path. The signal powers from the signal path and canceller output are combined using linear superposition at the summation symbol. The power detection element is used to provide feedback to the canceller so that it can adjust G_C in order to minimize the power in the detector. The jammer power transmitted through the signal path is given by $P_J G_S$, while the jammer power transmitted through the canceller is $P_J G_J G_C$. Perfect cancellation occurs when

$$(P_J G_S) + (P_J G_J G_C) = 0 \qquad (1)$$

or equivalently

$$G_C = -\frac{G_S}{G_J} \qquad (2)$$

Equation (2) represents the design philosophy used to compute the complex interference canceller gain G_C. If all of the jammer power were concentrated at the GPS L_1 frequency, then Equation (2) would predict perfect cancellation of the unwanted signal. It is more likely that jammer power will be distributed over a range of frequencies, centered at L_1, similar to the spread spectrum GPS signals themselves. In this case, perfect interference cancellation is not likely, but G_C may still be chosen so as to minimize the average jammer power transmission when summed over all frequencies.

Canceller Effectiveness

The canceller effectiveness E_c is defined as the ratio of jammer signal power into the summation junction divided by the residual unwanted signal power coming out of the summation junction and sent to the GPS receiver. In the above simplified case, the canceller effectiveness is infinite, since the power out of the junction was zero. To account for the spread-spectrum nature of the signals involved, the generic interference canceller diagram is modified as shown in Figure 2, where the input and transfer functions are functions of frequency, f_i. $P_J(f_i)$ denotes the jammer power in the i^{th} frequency bin, and $G_S(f_i)$ and $G_J(f_i)$ are the complex gains corresponding to the i^{th} frequency. Also note that there is now a bandpass filter centered at f_C. This bandpass filter represents the frequency-selective nature of the canceller. The canceller components that vary over frequency cannot be expected to vary in the same manner in both signal paths due to manufacturing differences and differences in the look angles through the signal and jammer antennas. This is the primary reason why cancellation of a CW tone is easier to achieve than cancellation of a broadband jammer. The perfect cancellation solution that is achievable at some discrete frequency is not possible when jammer power is distributed over frequency. Note that in Figure 2 the canceller solution G_C is not a function of frequency. The bandpass filter before the power detector illustrates how the canceller will create an optimal nulling at that discrete cancellation frequency f_C.

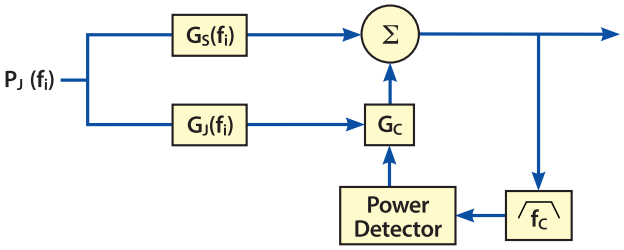

Figure 2—Interference Canceller Schematic Diagram

As before, we have $G_C = -\frac{G_S(f_C)}{G_J(f_C)}$, and the effectiveness at f_C is infinite. The effectiveness E_c at frequencies other than f_C is given by:

$$E_C(f_i) = \frac{P_J(f_i)G_S(f_i)}{P_J(f_i)\left(G_S(f_i) + G_J(f_i)G_C\right)} \quad (3)$$

Substituting for G_C yields:

$$E_C(f_i) = \frac{G_S(f_i)}{G_S(f_i) - G_J(f_i)\left(\frac{G_S(f_C)}{G_J(f_C)}\right)} \quad (4)$$

The effectiveness over the frequency range of interest is the total power into the summation junction divided by the total power out.

$$E_C = \frac{\sum P_J(f_i)G_S(f_i)}{\sum P_J(f_i)G_S(f_i) + G_J(f_i)G_C} \quad (5)$$

Canceller Center Frequency

The bandpass filter in the block diagram of Figure 2, is centered at some frequency f_C. This filter illustrates that the cancellation effect is optimized at a particular frequency. In this model, the frequency for maximum cancellation corresponds to the frequency where the input power is concentrated. If the jammer power is allowed to vary with frequency, then $P_J(f_i)$ will represent the power density versus frequency. The center frequency selected by the model corresponds to the centroid of this power over the band and is given by Equation (6). Note that this returns a frequency step (or bin) and not an actual frequency value.

$$i_c = \frac{\sum P_J(f_i)\cdot i}{\sum P_J(f_i)} \quad (6)$$

The canceller model considers twenty 1-MHz, wide-frequency bins, which represent the GPS P(Y) code spectrum. The bin centers are at 1566, 1567, 1568, …1585 MHz, corresponding to the frequencies at which antenna measurements were taken. The range of the input frequency space is defined as 1565.5 MHz to 1585.5 MHz. Any signals outside this range are considered outside the passband of the system.

ERGM must operate in the presence of both CW and broadband jammers. In this article, two power density functions representing two possible broadband modulation techniques are considered: a uniform power distribution and a *sinc*^{2} distribution that matches the shape of the radiated GPS spectrum. The sinc function is defined as: $\text{sinc}(x)=\sin(\pi x)/\pi x$. For the uniform density, the power per bin is $P_{BB}/20$, where P_{BB} is the total broadband power at the antenna. For the *sinc*^{2} power density, the power per bin is given by:

$$P_J(f_i) = \frac{P_{BB}W_i}{\sum_{i=0}^{19} W_i} \quad (7)$$

where the weights are defined as

$$W_i = \left(\frac{\sin\left(\frac{\pi}{10}\cdot(i-9.5)\right)}{\frac{\pi}{10}\cdot(i-9.5)}\right)^2, \; i = 0,1,.....19 \quad (8)$$

Note that the total power is the same for the uniform and *sinc*^{2} modulations.

Antenna Characteristics

Antenna data were taken at various azimuth and elevation angles on a set of five representative patch antennas in twenty 1-MHz steps around the GPS center frequency. The elevation angles were chosen to create *angle pairs*, so that the lines of sight from the top and bottom antennas toward a jammer location would appear as seen in Figure 3. The angles measured were 45, 60, 75, 90, 105, 120, and 135 degrees, measured from a line normal to the projectile axis. Note in the elevation view of Figure 3 that the angle for the top antenna (G_S) is always equal to 180° minus the angle for the lower antenna (G_J). The angle pairs from the measured data are 45°–135°, 60°–120°, 75°–105°, and 90°–90°.

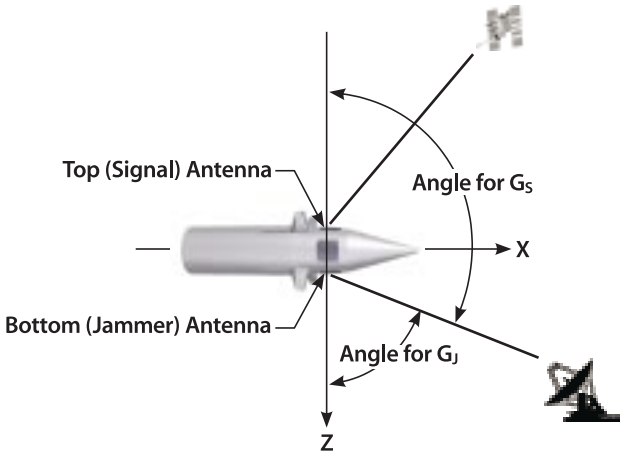

Figure 3—GPS Interference Cancellation System Antenna Geometry

Interference Cancellation System Integration

In the NSWCDD system model, the calculation of carrier-to-noise power ratio (C/N_o) for a satellite in the presence of a jammer is a three-step process:[1]

1. Calculate the jammer-to-signal power ratio (J/S) based on geometry, jammer power, polarization, and antenna gain,
2. Calculate the carrier-to-noise ratio C/N_o for each satellite based on the antenna gain and receiver noise characteristics,
3. Calculate the effective C/N_o based on the C/N_o and J/S.

Jammer immunity is derived from both the canceller and the ratio of the antenna gains toward the satellite and jammer. When considering the effect of the canceller on the GPS signal path, the model incorporates a canceller noise floor that can dominate the GPS signal. For simplicity, the present model assumes that the canceller circuitry increases the receiver noise floor from 4 to 7 dB when the circuit is active.

One can combine the canceller model with the C/N_o calculation by first calculating the lines-of-sight to the jammers and satellites. The canceller effectiveness module is then used to calculate the interference cancellation for a given jammer look angle.

When both CW and broadband jammers are considered simultaneously, jammer-to-signal power ratio, J/S, associated with each type of jammer is calculated independently, based upon both CW and broadband effectiveness according to:

$$\frac{J_{CW}}{S} = 10\log(P_{CW}) + G_S(az_J, el_J)_{CW} - 20\log\left(\frac{4\pi}{c} R_{CW}\ f\right) - S_0 - G_S(az_S, el_S) - E_{CW}$$

$$\frac{J_{BB}}{S} = 10\log(P_{BB}) + G_S(az_J, el_J)_{BB} - 20\log\left(\frac{4\pi}{c} R_{BB}\ f\right) - S_0 - G_S(az_S, el_S) - E_{BB} \quad (9)$$

where

J_{CW}/S = CW jammer to signal power ratio (dB)
R_{CW} = range to CW jammer (m)
J_{BB}/S = broadband jammer to signal power ratio (dB)
R_{BB} = range to broadband jammer (m)
c = speed of light (m/s)
f = carrier frequency (Hz) (L_1 or L_2)
S_0 = received GPS signal strength at antenna (dBw)
$G_S(az_J, el_J)$ = gain of top antenna towards jammer (dBi)
$G_S(az_S, el_S)$ = gain of top antenna towards satellite (dBi)
P_{CW} = CW jammer EIRP (watts)
P_{BB} = broadband jammer EIRP (watts)
E_{CW} = canceller CW effectiveness (dB)
E_{BB} = canceller broadband effectiveness (dB)

Note all powers are referenced to the antenna and include the appropriate attenuations over the transmitted path lengths. The carrier-to-noise ratio, C/N_o, is computed for each satellite by Reference 1:

$$\frac{C}{N_0} = S_0 + G_S(az_S, el_S) - 10\log(kT_0) - N_f - L \quad (10)$$

where

$10\log(k \cdot T_0)$ = thermal noise density (dBw-Hz)
L = implementation loss (dBw)
N_f = noise figure (4 dB if canceller is off, 7 dB if canceller is on)

The equivalent C/N_0 is computed as:

$$\left(\frac{C}{N_0}\right)_{eq} = \frac{1}{\frac{1}{C/N_0} + \frac{J_{CW}/S}{Q_{CW}R_C} + \frac{J_{BB}/S}{Q_{BB}R_C}} \qquad (11)$$

where Q is the spread-spectrum processing gain adjustment factor determined by the type of jammer scenario modeled:

Q_{CW} = 1.0 (narrowband or CW jammer)
Q_{BB} = 1.5 (broadband uniform jammer)
Q_{BB} = 2.0 (broadband $sinc^2$ noise jammer)

and R_C is the GPS PRN code chipping rate (chips/sec).

Multiple Jammer Sources

The case of multiple jammers may be treated as shown in the diagram of Figure 4. Let the jammer power be denoted by P_{Jk}, where k=1, 2, …n. Let G_{SJk} be the signal path complex gain associated with the k^{th} jammer input, and G_{JJk} be the jammer path

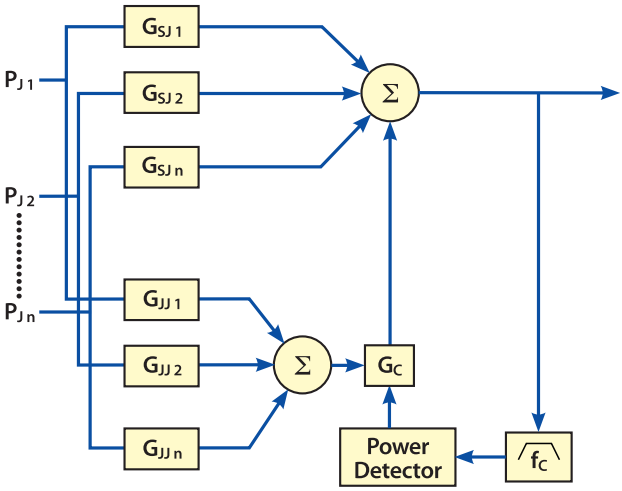

Figure 4—Treatment of Multiple Jammers

complex gain for that input. As before, the gains G_S and G_J will depend on the antenna response over frequency in the direction of the jammer. The center frequency calculation for the bandpass filter must take into account all the power entering into the jammer path from all jammer sources. Again, note that the result is in terms of bin number and not actual frequency.

$$i_c = \sum_{k=1}^{n}\left(\frac{\sum_{i=1}^{20} P_{Jk}(f_i)G_{JJk}(f_i)i}{\sum_{i=1}^{20} P_{Jk}(f_i)G_{JJk}(f_i)}\right) \qquad (12)$$

The complex, interference-canceller gain to yield optimal nulling is calculated at the frequency corresponding to the calculated centroid bin

$$G_C = -\frac{\sum P_{Jk}(f_C)G_{SJk}(f_C)}{\sum P_{Jk}(f_C)G_{JJk}(f_C)} \qquad (13)$$

This is the canceller complex gain that cancels out the composite signal due to all jammers at the centroid frequency. It is the same complex gain that is applied to each jammer independently at each frequency. Therefore, the canceller effectiveness for the k^{th} jammer is given by:

$$E_k = \frac{\sum P_{Jk}(f_i)G_{SJk}(f_i)}{\sum P_{Jk}(f_i)G_{SJk}(f_i) + G_{JJk}(f_i)G_C} \qquad (14)$$

This *per jammer effectiveness* is used in the calculation of C/N_o as before, except that J/S becomes J_k/S—the effect of the k^{th} jammer—and the J/S in the effective C/N_o calculation would be replaced with J_{TOTAL}/S.

Gain and Phase Tracking

A fundamental factor in the effectiveness of the interference cancellation technique is the gain and phase tracking characteristics of the antenna pair. The gain and phase of the two antennas toward the source need not be equal. Recall that the canceller circuit adjusts to account for differences at the

frequency of maximum cancellation. However, the gain and phase variation of the two antennas with frequency (expressed as dB/MHz or deg/MHz) must be similar, within a specified tolerance. For instance, if the gain and/or phase increases on the jammer antenna, then the gain and/or phase on the signal antenna must change by the same amount, or a degradation in the effectiveness will occur. One goal of this modeling effort is to provide a tool for evaluating canceller performance for variations in antenna gain and phase tracking.

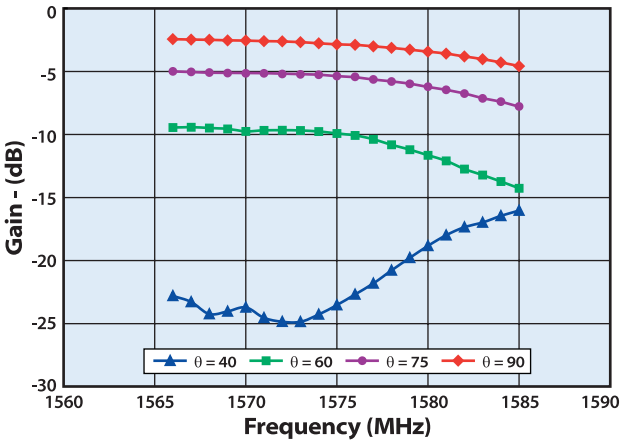

Figure 5—RHCP Antenna Gain vs. Frequency

CANCELLER AND NAVIGATION SYSTEM PERFORMANCE EVALUATION

Canceller Static Effectiveness Evaluation

Following the development of the interference cancellation model, calculations of canceller effectiveness were made to assess its antijam performance divorced from navigation system issues. Canceller effectiveness is primarily a function of jammer frequency, power distribution, antenna gain, and jammer polarization. Jammer power and distribution were modeled for both CW and broadband jammers. Jammer power spectral density was also varied, such that perfect cancellation of the CW jammer was not realized except for highly idealized cases.

The antenna data used in the evaluation were collected as vertical and horizontal polarization complex gains. This allows the response to any linear or circular polarized signal to be synthesized by combining the vertical and horizontal responses. Variations in antenna gain with frequency and elevation angle for a right-hand, circularly-polarized (RHCP) signal are shown in Figure 5. Note that elevation angle here refers to the angle between the projectile-jammer line of sight and the projectile z-axis as shown in Figure 3.

It is important to note that the system antijam performance is not determined by the canceller alone. At any given elevation angle, the total system effectiveness is influenced by both the canceller effectiveness, E_C, and by the ratio of the gain of the top antenna toward the satellite to the gain of the top antenna toward the jammer. The latter is referred to as the *shadowing factor* or *shadowing effectiveness*, E_S, and arises from body masking and the natural directional nature of the upper antenna patch.

Refer to the diagram in Figure 6, and define the *effective J/S ratio* as the residual jammer power out of the canceller circuit divided by the GPS power in the main signal path:

$$(J/S)_{EFF} = \frac{P_\varepsilon}{P_S G_{SS}} \qquad (15)$$

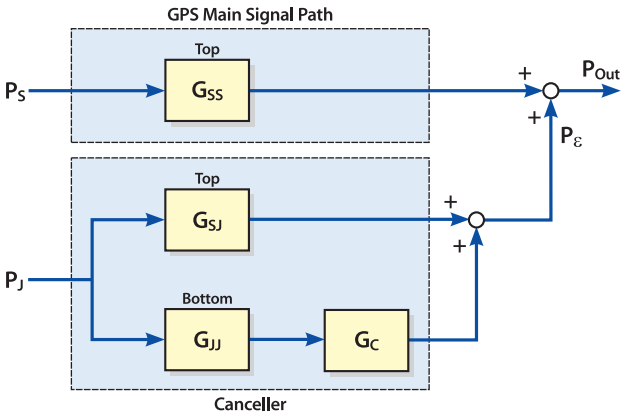

Figure 6—Cancellation System Interaction with GPS Signal Path

The canceller effectiveness, $E_{C,}$ is defined by the equation:

$$E_C = \frac{P_J G_{SJ}}{P_\varepsilon} \quad (16)$$

Note when the cancellation is perfect, P_ε is zero and E_C is infinite. The shadowing factor, $E_{S,}$ is defined as:

$$E_S = \frac{G_{SS}}{G_{SJ}} \quad (17)$$

Substituting Equations (16) and (17) into (15) gives:

$$(J/S)_{EFF} = \frac{P_J}{P_S E_C E_S} \quad (18)$$

Now define *total system antijam effectiveness*, $E_{T,}$ as:

$$E_T = E_C E_S \quad (19)$$

Substituting (19) into (18), and letting $P_J/P_S = (J/S)_{NOM}$ gives:

$$(J/S)_{EFF} = \frac{(J/S)_{NOM}}{E_T} \quad (20)$$

The results in Equations (19) and (20) illustrate two important features of the antijam system. First, total effectiveness is the direct combination of canceller and shadowing effectiveness. Second, the nominal J/S is directly reduced by E_T to give the effective system J/S.

Figures 7 and 8 display typical canceller broadband effectiveness and shadowing for a sinc^2 broadband jammer. At the elevation angles where the canceller performance is predicted to be low, the shadowing effect is seen to be high, yielding a more uniform total system effectiveness variation with elevation angle. In addition to elevation angle, signal polarization can have a significant effect on canceller total effectiveness as shown in Figure 8. Here canceller broadband effectiveness is displayed for several assumed jammer polarizations, and the resulting variations in effectiveness are seen to be as large as 10–15 dB.

Canceller System Level Evaluation

Since ERGM is still in the early stages of development, a number of design and operational issues relating to navigation system performance are currently being addressed. Therefore, a 6-DOF flight simulation was developed by NSWCDD to examine aerodynamics, guidance, and control issues. In addition, a Monte Carlo navigation simulation[2, 3] was developed to evaluate the performance of the GPS-aided navigation system. The 6-DOF model

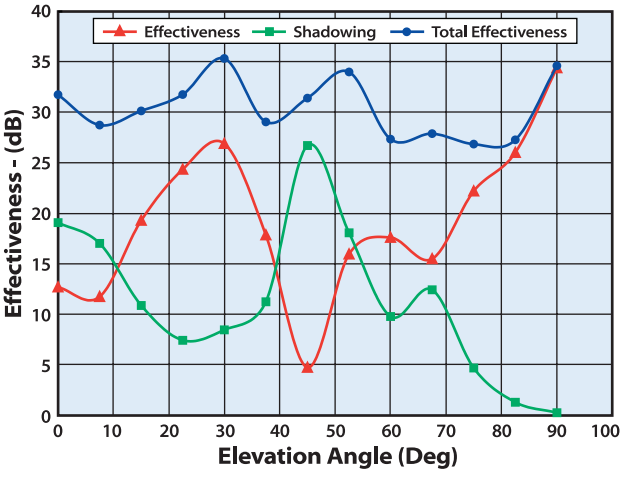

Figure 7—Canceller Effectiveness and Shadowing for RHCP Sinc^2 Broadband Jammer

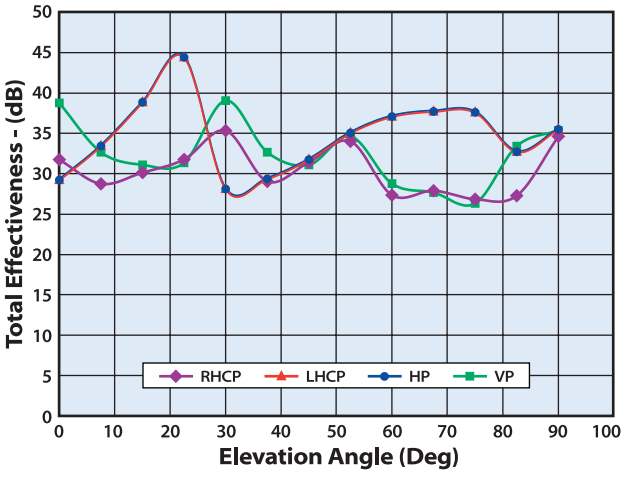

Figure 8—System Total Effectiveness for Various Jammer Polarizations

was used to compute trajectory and IMU data along two notional ERGM trajectories[4] of 40- and 60-NM range shown in Figure 9. The trajectories were generated using an initial velocity of 2790 ft/s, with airframe roll control established at 3.0 s into the flight with two canards deployed. Table 1 contains ERGM trajectory descriptive data, and Table 2 contains GPS/INS system errors for the study.

True position, velocity, attitude, accelerometer, and gyro data were recorded along the two trajectories. The generic antijam canceller algorithm and navigation system performance were evaluated under conditions similar to those assumed in previous studies.[4] Statistical results are based upon 50-sample Monte Carlo sets. Each random sample is created by corrupting perfect IMU measurements with IMU errors taken from normal distributions associated with Table 2. Acquisition of the GPS signal is assumed when the equivalent carrier to noise ratio $(C/N_o)_{eq}$ is above 30 dB. Once acquired, it is further assumed that the GPS receiver maintains carrier phase track (State 5) so long as the $(C/N_o)_{eq}$ is above 25 dB, while code tracking (State 3) is assumed when $(C/N_o)_{eq}$ remains above 16 dB.

The benefits derived from the active interference cancellation system are clearly demonstrated in Figures 10–19. When active interference cancellation is not used, the resulting $(C/N_o)_{eq}$ and total (J/S) environment are as shown in Figures 10 and 11 for the 40-NM trajectory, and Figures 15 and 16 for the 60-NM trajectory. These calculations assume a 1-kW CW jammer and a 100-W $sinc^2$ broadband jammer collocated at the target, with the CW power concentrated in the center of the band at 1575.5 MHz. GPS acquisition is allowed after 8 s, and where possible, tracking is maintained on up to eight active channels. Without active interference cancellation, these results indicate that GPS acquisition is very unlikely for both 40- and 60-NM trajectories, with all channels never exceeding the acquisition threshold of 30 dB. However, when active interference cancellation is used, all channels acquire and maintain track until very late in both trajectories, as seen in Figures 12 and 17 for the 40- and

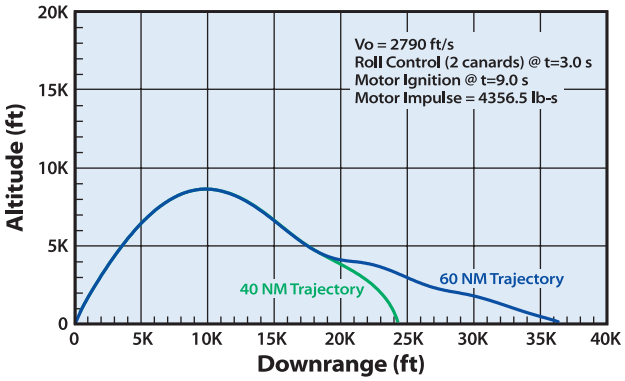

Figure 9—Notional Flyout Trajectories

Table 1—ERGM Trajectory Characteristics

Range (NM)	QE (deg)	γ_F (deg)	Guidance Activate (s)	Time of Flight (s)
40	60	-70	74.55 (apogee)	201.52
60	60	-30	74.55 (apogee)	382.52

Table 2—Initial INS Errors

Navigation System Error	3-σ Value		
	Roll(X)	Pitch(Y)	Yaw(Z)
Initial Position Error (m)	100	100	100
Initial Velocity Error (m/sec)	10	10	10
Initial Attitude Error (deg)	20	3	3
Gyro Drift (deg/hr)	50	50	50
Gyro Scale Factor (ppm)	10,000	10,000	10,000
Gyro Random Walk (deg/rt-hr)	0.3	0.3	0.3
Gyro Misalignment (mrad)	0.5	0.5	0.5
Accelerometer Bias (mg)	10	10	10
Accelerometer Scale Factor (ppm)	700	700	700
Accelerometer Noise (mg)	1.87	1.87	1.87
Accelerometer Misalignment (mrad)	0.325	0.325	0.325

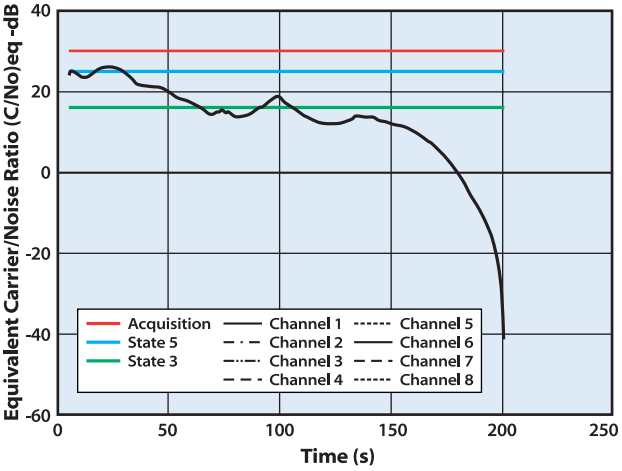

Figure 10—$(C/N_o)_{eq}$ Without Interference Cancellation: 40-NM Trajectory

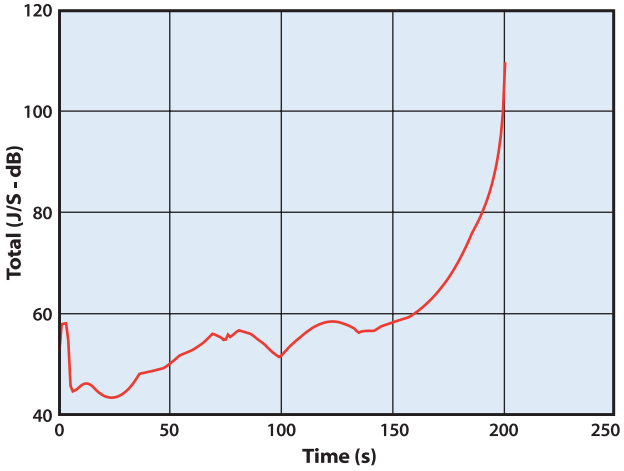

Figure 11—Total (J/S) Without Interference Cancellation: 40-NM Trajectory

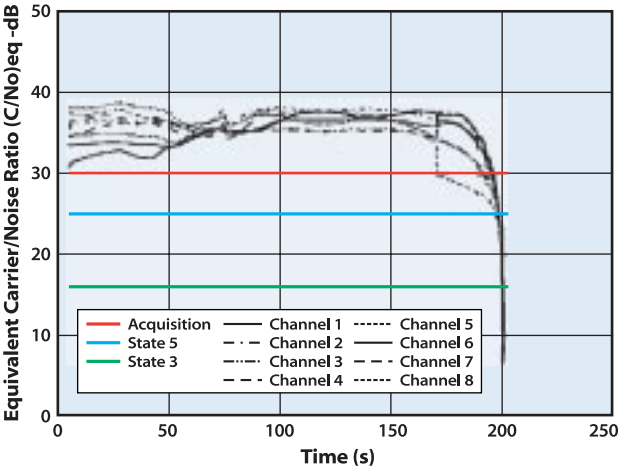

Figure 12—$(C/N_o)_{eq}$ With Active Interference Cancellation: 40-NM Trajectory

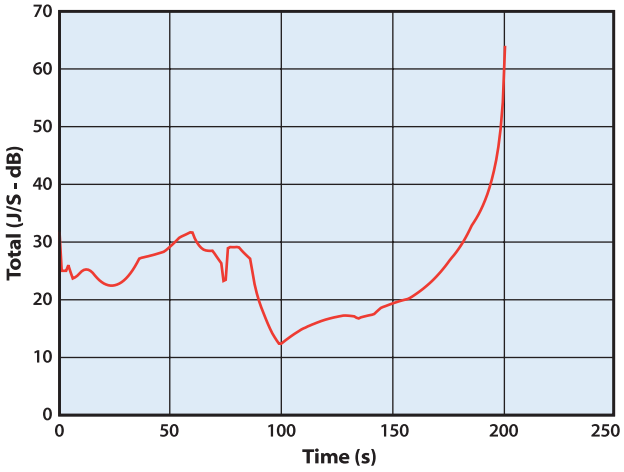

Figure 13—Total (J/S) With Active Interference Cancellation: 40-NM Trajectory

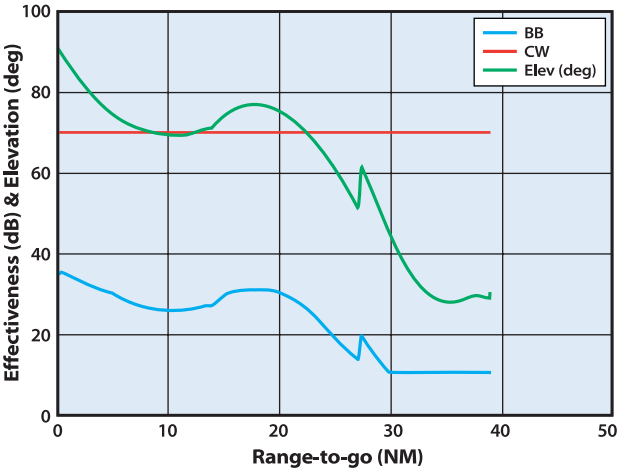

Figure14—Antenna Elevation and Canceller Effectiveness: 40-NM Trajectory

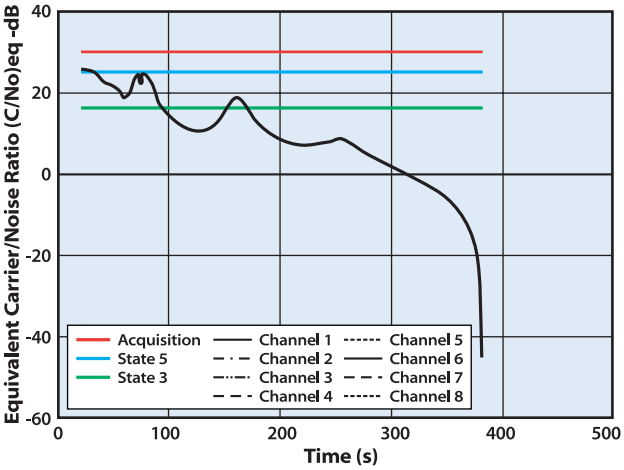

Figure 15—$(C/N_o)_{eq}$ Without Active Interference Cancellation: 60-NM Trajectory

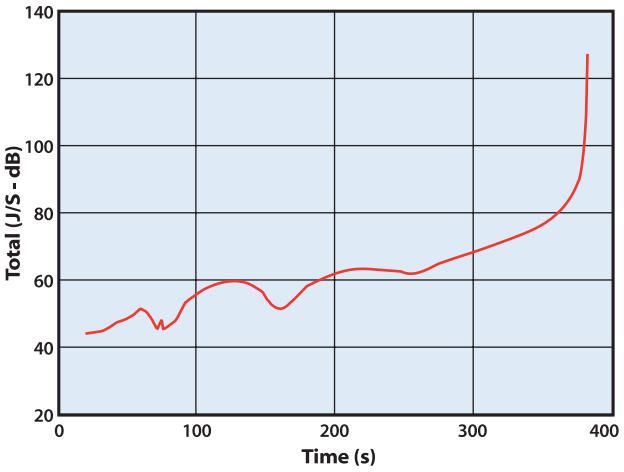

Figure 16—Total (J/S) Without Active Interference Cancellation: 60-NM Trajectory

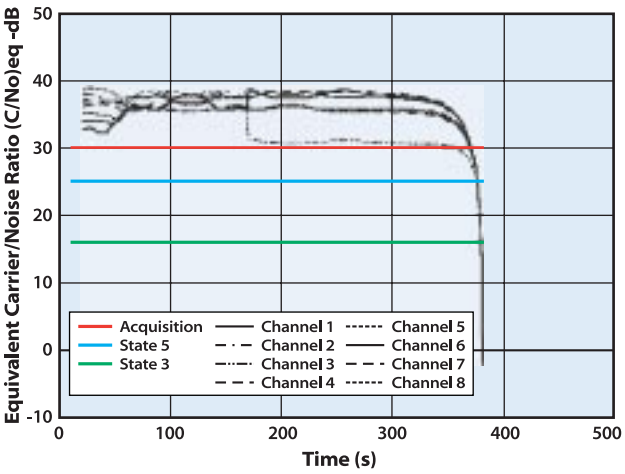

Figure 17—$(C/N_o)_{eq}$ With Active Interference Cancellation: 60-NM Trajectory

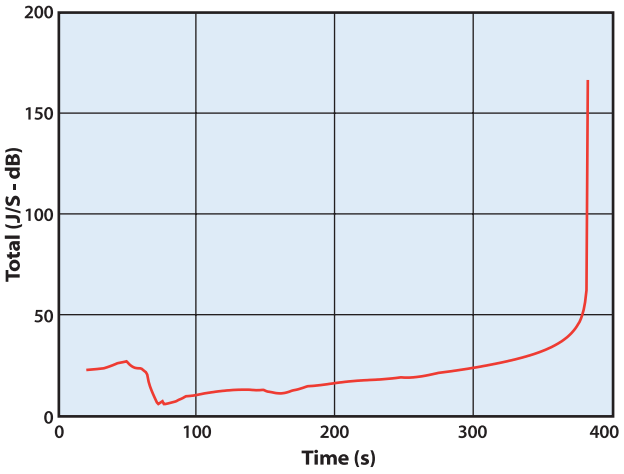

Figure 18—Total (J/S) With Active Interference Cancellation: 60-NM Trajectory

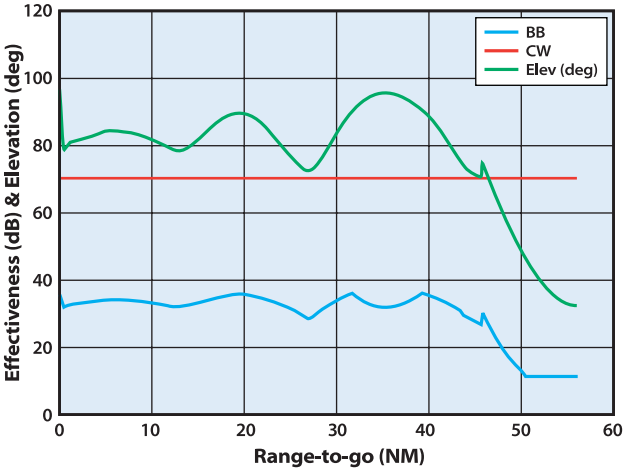

Figure 19—Antenna Elevation and Canceller Effectiveness: 60-NM Trajectory

60-NM trajectories, respectively. Canceller performance is further evidenced by the effectiveness plots of Figures 14 and 19, where the CW jamming is shown to be virtually removed (E_{CW} = 70 dB), and the broadband effectiveness remains in excess of 20 dB for a considerable portion of the flight. The correlation of effectiveness with elevation angle is also shown in these figures.

To further evaluate the robustness of the interference cancellation technique, calculations were also made simulating a 10-kW CW jammer and a 100-W broadband jammer with a sinc^2 power distribution. Figure 20 shows results when the jammer CW frequency is placed at the center of the passband (1575.5 MHz). In Figure 21, the CW frequency was placed at the extreme lower edge of the canceller passband (1565.5 MHz). This situation simulates a somewhat unfavorable condition in that the power spectral averaging employed by the canceller allows the maximum amount of jammer power into the signal path. The $(C/N_o)_{eq}$ for all eight channels was plotted along the 40-NM trajectory together with the assumed thresholds for acquisition and for code and carrier phase tracking. Even in the more severe case of Figure 21, the computed $(C/N_o)_{eq}$ is seen to remain well above the acquisition threshold of 30 dB for most of the trajectory. State 5 carrier phase tracking is maintained on seven active channels until 8 s before impact, while State 3 code

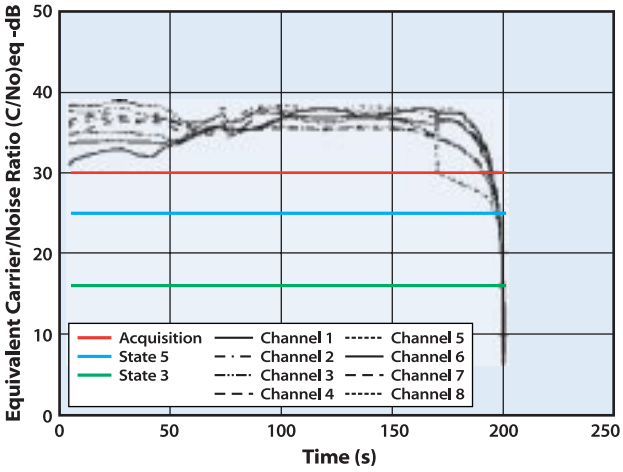

Figure 20—$(C/N_o)_{eq}$ With Active Interference Cancellation: CW Frequency @ 1575.5 MHz

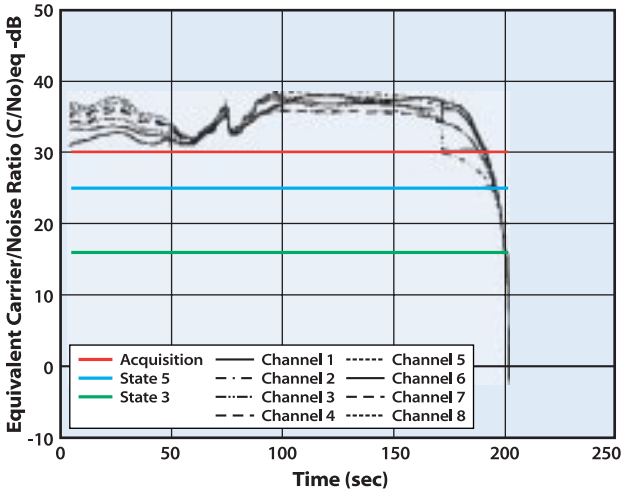

Figure 21—$(C/N_o)_{eq}$ With Active Interference Cancellation: CW Frequency @ 1565.5 MHz

tracking is maintained on eight channels until 3 s before impact.

Monte Carlo Navigation Performance Evaluation

In order to assess the ability of the navigation system to perform in a countermeasures environment, a detailed model of the GPS/INS described in Reference 4 was used in combination with the interference cancellation model. Monte Carlo navigation simulations were run using the INS initialization and instrument errors shown in Table 2, and the 600 Hz IMU data generated by the NSWCDD 6-DOF simulation. Statistical navigation performance data along the 40-NM, medium-range trajectory were based upon 50 Monte Carlo replications, with all input navigation system errors normally distributed. While eight satellites were tracked throughout the flight, only six channels were used for INS aiding. The resulting GPS dilution of precision at the time of launch was calculated to be 2.9. The time of launch in relation to the GPS week was not randomly chosen, but was held constant at the beginning of week 848.

Figures 22–30 show typical behavior of the GPS-aided navigation system and the benefits derived from the active interference cancellation when operating in a severe jamming environment. Simulated conditions included the combined jamming of a 10-kW CW jammer operating at 1565.5 MHz (band edge) and a 100-W broadband $sinc^2$ jammer, both collocated at the target. Plotted in the figures are the mean error, and the mean ± 1 standard deviation (σ), computed for the 50 trajectory ensemble. Under these severe jamming conditions, the active interference cancellation system allows fast GPS acquisition and uninterrupted GPS aiding for virtually the entire trajectory, with loss of code tracking occurring approximately 3 s prior to impact. This results in excellent navigation system accuracy, where the maximum position error is below 3 m and the maximum

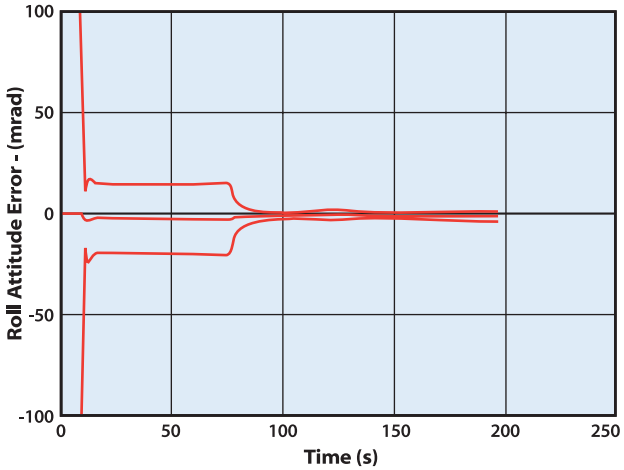

Figure 22—Roll Attitude Error - 40-NM Trajectory, 10 kW CW & 100-W Broadband Jammer

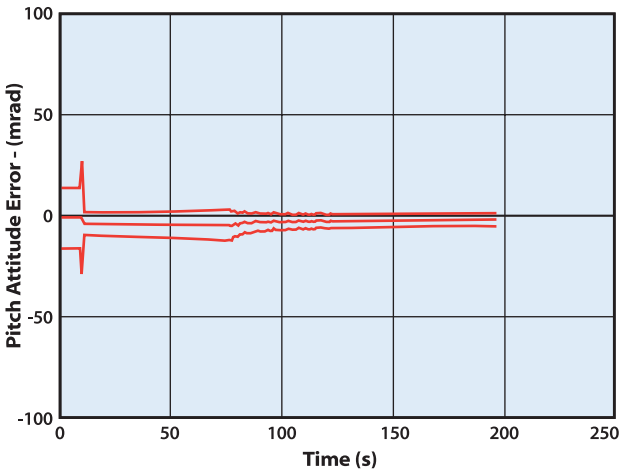

Figure 23—Pitch Attitude Error: 40-NM Trajectory, 10 kW CW & 100-W Broadband Jammer

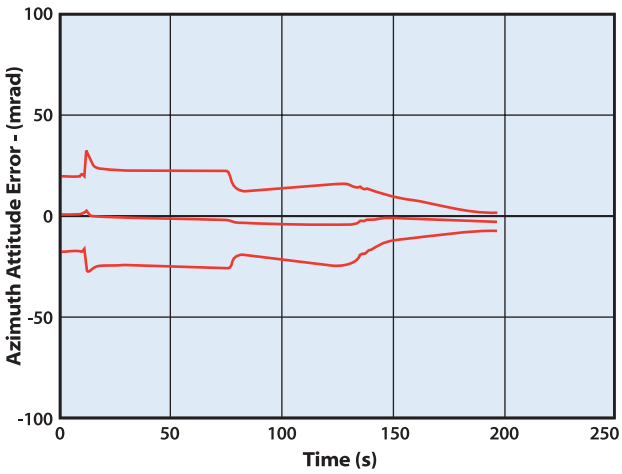

Figure 24—Azimuthal Attitude Error: 40-NM Trajectory, 10 kW CW & 100-W Broadband Jammer

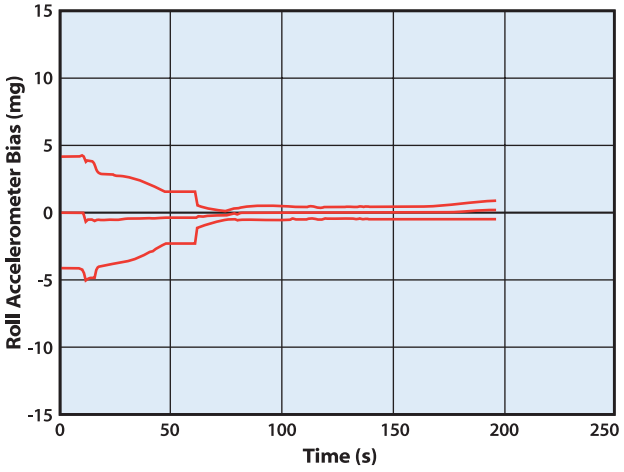

Figure 25—Roll Accelerometer Bias: 40-NM Trajectory, 10 kW CW & 100-W Broadband Jammer

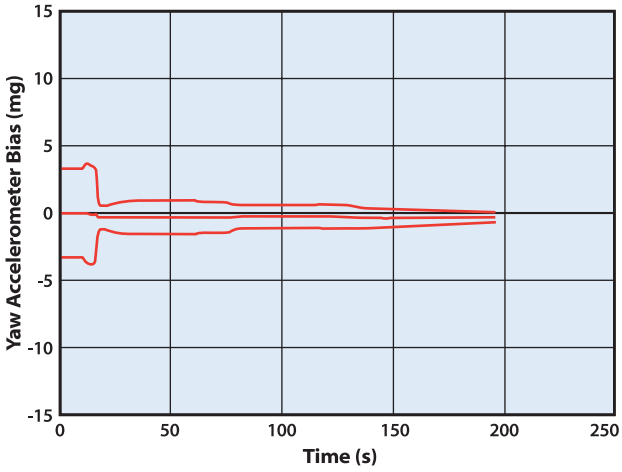

Figure 26—Yaw Accelerometer Bias: 40-NM Trajectory, 10 kW CW & 100-W Broadband Jammer

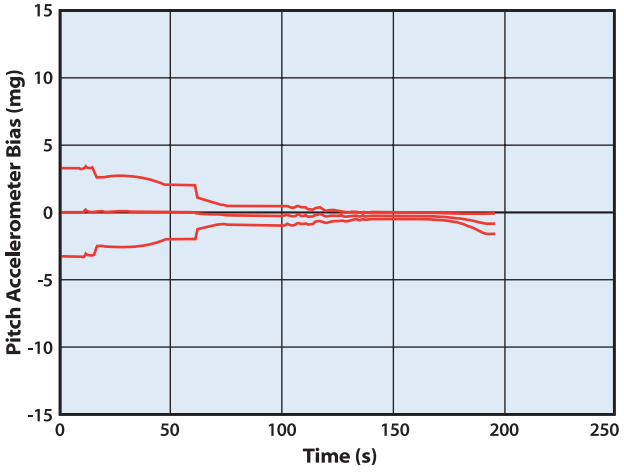

Figure 27—Pitch Accelerometer Bias Error: 40-NM Trajectory, 10 kW CW & 100-W Broadband Jammer

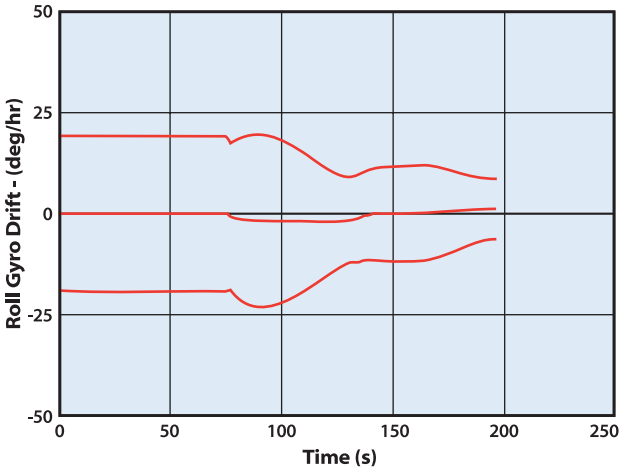

Figure 28—Roll Gyro Drift: 40-NM Trajectory, 10 kW CW & 100-W Broadband Jammer

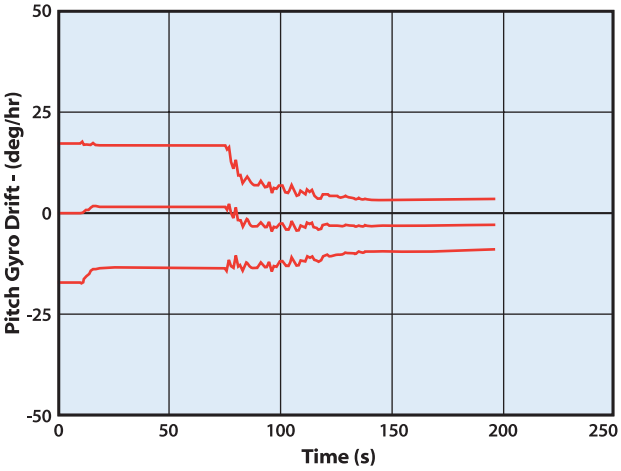

Figure 29—Pitch Gyro Drift: 40-NMTrajectory, 10 kW CW & 100-W Broadband Jammer

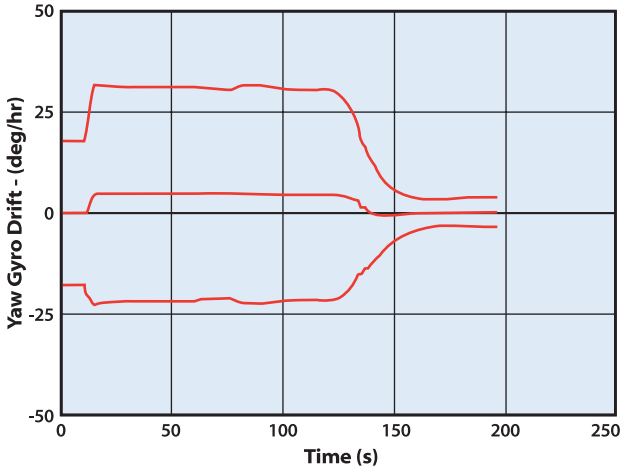

Figure 30—Yaw Gyro Drift: 40-NM Trajectory, 10 kW CW & 100-W Broadband Jammer

velocity error is less than 1 m/s along the downrange, cross-range, and vertical axes.

Other navigation system errors were similarly reduced. Projectile attitude errors, shown in Figures 22–24, are slow to converge until near apogee, where the projectile glide sequence is activated, and the attitude error estimates respond to the applied 1-G specific force. The roll, pitch, and yaw errors are reduced dramatically from the large initial values shown in Table 2. Projectile attitude errors are more difficult to estimate because they are not directly measurable but are inferred from multiple observations through the use of a Kalman navigation filter. Based on the limited Monte Carlo sample, the navigation filter reduces 1-σ roll and pitch errors to less than 5 mrad just before impact, while the 1-σ yaw attitude error (least observable) is reduced to less than 10 mrad.

The ability of the filter to calibrate the inertial instruments during GPS/INS aiding is demonstrated by the data of Figures 25–30, where the residual accelerometer bias and gyro drift errors are shown along the 40-NM trajectory. Figures 25–27 show that the 1-σ accelerometer bias errors are reduced to less than 2 milli-G's just before impact. Gyro drift errors were found to be somewhat less observable as indicated by the data in Figures 28–30. Despite this reduced observability, the data show that the 1-σ pitch, yaw, and roll gyro drifts were reduced to less than 10 deg/hr just prior to GPS loss of lock.

SUMMARY

A generic, Navy-derived interference cancellation algorithm was developed and integrated into an existing GPS/INS navigation simulation. These were then used with a 6-DOF simulation of an early developmental ERGM configuration to evaluate system antijam performance. Several representative trajectories in various jamming environments were analyzed for both CW and broadband jammers. Canceller effectiveness and its sensitivity to jammer power, frequency, spectral distribution, polarization, and trajectory geometry were determined. The antijam immunity made possible by the use of the canceller greatly enhanced the ability of the GPS/INS navigator to remove IMU and navigation errors during flight. For the notional ERGM trajectories and jamming scenarios studied in this article, GPS/INS performance was found to be quite satisfactory when the interference canceller was operating. Without the canceller, GPS acquisition was inhibited, and navigation performance was severely degraded. The results of this study are preliminary, and will be refined as new information

becomes available. Continued validation of the cancellation system model using hardware and experimental data is essential to gaining confidence in model predictions.

ACKNOWLEDGMENTS

The authors would like to thank Ken Nichols of NSWCDD for his contributions to the model implementation, Eldon Gordon of Raytheon Systems Company for assistance in interpreting the antenna data, and Scott Williams and Bob Flanagan of American Nucleonics Corporation for valuable insights into the theory and operation of noise suppression systems. Thanks also to Steve Malyevac, Craig Phillips, and Steve Rowles of NSWCDD, who developed the ERGM 6-DOF flight simulation and provided data used in this article.

REFERENCES

1. Ward, P.W., "GPS Receiver RF Interference Monitoring, Mitigation, and Analysis Techniques," *NAVIGATION, Journal of the Institute of Navigation*, Vol. 41, No. 4, pp. 367-391, Winter, 1994-95.

2. Ohlmeyer, E.J.; Pepitone, T.R.; Miller, B.L.; Malyevac, D.S.; Bibel, J.E. and Evans, A.G., *System Modeling and Analysis of GPS/INS For Extended Range Guided Munitions*, Naval Surface Warfare Center, Dahlgren Division, NSWCDD/TR-96/159, Dahlgren, VA, May 1997.

3. Ohlmeyer, E.J.; Pepitone, T.R.; Miller, B.L.; Malyevac, D.S.; Bibel, J.E. and Evans, A.G., "GPS-Aided Navigation System Requirements for Smart Munitions and Guided Missiles," AIAA Guidance, Navigation, and Control Conference, New Orleans, LA, Aug 1997.

4. Ohlmeyer, E.J.; Pepitone, T.R. and Miller, B.L., "Assessment of Integrated GPS/INS for the EX-171 Extended Range Guided Munition," AIAA Guidance, Navigation and Control Conference, Boston, MA, Aug 1998.

THE AUTHORS

MR. GEORGE C. WILES IV

Mr. George C. Wiles IV received a B.S. degree in electrical engineering from Virginia Tech in 1983. He spent 13 years working in radar fuzing and GPS position location devices for artillery at the Army Research Laboratory (ARL). In 1995 he won the Army R&D Achievement Award and ARL Achievement Award for developing the GPS Registration Fuze system, which uses rugged GPS transponders to track artillery projectiles. This work was the basis for the continuing Low-Cost Competent Munition program in the Army. Mr. Wiles joined NSWCDD in 1996, where he presently serves as ERGM system engineering and guidance team lead. He is a member of the Institute of Navigation and the Association of Old Crows.

MR. ERNEST J. OHLMEYER

Mr. Ernest J. Ohlmeyer joined NSWCDD (then the Naval Weapons Lab) in 1968 after receiving a B.S. degree in physics from Loyola University. In 1982, he obtained an M.S. degree in engineering science from the Naval Postgraduate School. His main activities have emphasized the analysis of guided missile and projectile systems including the Tomahawk and Standard missiles, ERGM, and the SM-3 Navy Theaterwide Missile System. Mr. Ohlmeyer has been principal investigator on several independent research and weapons technology programs. He is currently group leader for flight dynamics, guidance, and control in the Missile Systems Engineering Branch at NSWCDD. Over the past 4 years, he has led a multidepartment GPS/INS analysis team that has supported SM-3, ERGM, Tomahawk, and other programs. Mr. Ohlmeyer's technical interests include: robust and nonlinear control, missile guidance algorithms, system design optimization, and applications of GPS/INS. Mr. Ohlmeyer is an Associate Fellow of the American Institute of Aeronautics and Astronautics (AIAA).

THE AUTHORS (CONTINUED)

DR. THOMAS R. PEPITONE

Dr. Thomas R. Pepitone received a B.S. degree in aerospace engineering from the Georgia Institute of Technology in 1965, and M.S. and Ph. D. degrees in aerospace engineering from the University of Virginia in 1968 and 1977, respectively. From 1968 through 1986, he was employed by NSWCDD and participated in several research and development programs ranging from unguided munitions to tactical and strategic missile systems. In 1990 he founded Aerospace Technology, Inc., an engineering consulting firm specializing in missile guidance, navigation, and control. Dr. Pepitone is a member of the Institute of Electrical and Electronics Engineers and a senior member of the AIAA.

MR. GARY L. SITZMAN

Mr. Gary L. Sitzman is a senior analyst at NSWCDD. He has written numerous technical reports in the areas of missile trajectory simulation, system accuracy, and gravity modeling algorithms. Currently, his area of work involves developing new applications for existing strategic missiles. He graduated from Westmar College in 1964 with a B.S. in mathematics. He later received an M.S. from the University of South Dakota and came to NSWCDD in November 1966. In December 1992 he was the recipient of the Navy Meritorious Civilian Service Award. He is also a member of the AIAA.

THE AUTHORS (CONTINUED)

MR. B. LARRY MILLER

Mr. B. Larry Miller received a B.A. degree in mathematics and physics from Western Kentucky University in 1967 and an M.A. degree in mathematics from the University of Louisville in 1971. He was a staff meteorologist at Vandenberg Air Force Base until 1972 and has since been employed at NSWCDD. Since 1974, he has worked on numerous aspects of the GPS, including satellite constellation design, concept evaluation of ground and space applications, and development of the first space-borne GPS navigational unit. He is also a senior member of the Institute of Navigation.

MS. PAULA K. KHOE

Ms. Paula K. Khoe earned a B.S. degree in physics from Furman University in 1996 and an M.A.E. degree in aerospace engineering from Auburn University in 1997. Ms. Khoe has been working in GPS applications since 1996 and has been employed at NSWCDD since 1997. She is a member of the AIAA.